## EDGE ARTICLE

# Radiation-induced aerobic oxidation *via* solvent-derived peroxyl radicals†

Yang Xu, ‡[a] Bo-Shuai Mu,‡*[a] Zhiyu Tu, [a] Weiqiu Liang,[a] Jiahao Li,[a] Ziyang Sang [a] and Zhibo Liu *[abcd]

Oxidation is a fundamental transformation in synthesis. Developing facile and effective aerobic oxidation processes under ambient conditions is always in high demand. Benefiting from its high energy and good penetrability, ionizing radiation can readily produce various reactive species to trigger chemical reactions, offering another option for synthesis. Here, we report an ionizing radiation-induced aerobic oxidation strategy to synthesize oxygen-containing compounds. We discovered that molecular oxygen ($O_2$) could be activated by reactive particles generated from solvent radiolysis to produce solvent-derived peroxyl radicals ($R_{sol}OO\cdot$), which facilitated the selective oxidation of sulfides and phosphorus(III) compounds at room temperature without catalysts. Density functional theory (DFT) calculations further revealed that multiple $R_{sol}OO\cdot$ enable the oxidation reaction through an oxygen atom transfer process. This aerobic oxidation strategy broadens the research scope of radiation-induced chemical transformations while offering an opportunity to convert nuclear energy into chemical energy.
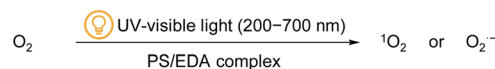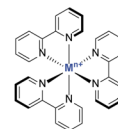
## Introduction

Oxidation reactions are among the most widespread transformations in synthesis.[1] With the growing interest in green synthesis and sustainable chemistry, molecular oxygen ($O_2$) is regarded as an ideal oxidant due to its good natural abundance and high cost-effectiveness, making it a superior choice for synthesizing oxygen-containing compounds. Utilizing oxygen instead of classical oxidants not only eliminates the need for stoichiometric reagents, but also avoids harsh reaction conditions and the production of potentially toxic waste.[2] Emerging as an environmentally friendly approach, the photochemical aerobic oxidation strategy under ambient conditions has garnered extensive attention in recent years and continues to evolve.[3] In this strategy, triplet oxygen with relatively low reactivity is usually activated by photosensitizers (PSs, *e.g.*, transition metal complexes and π-conjugated aromatic dyes) or electron donor–acceptor (EDA) complexes to produce singlet oxygen ($^1O_2$) or superoxide anion radicals ($O_2{}^{\cdot-}$) for subsequent reactions (Scheme 1a).[4] Nonetheless, the diversity of reactive oxygen species (ROS) remains limited, and the incorporation of catalysts
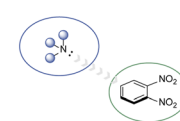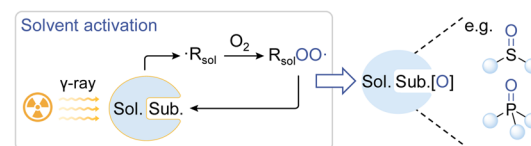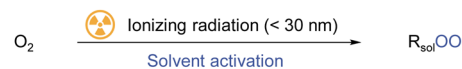


**Scheme 1** Solvent-derived peroxyl radicals enable radiation-induced aerobic oxidation. UV = ultraviolet, Sol. = solvent, and Sub. = substrate.

*[a]Beijing National Laboratory for Molecular Sciences, Radiochemistry and Radiation Chemistry Key Laboratory of Fundamental Science, Key Laboratory of Bioorganic Chemistry and Molecular Engineering of Ministry of Education, College of Chemistry and Molecular Engineering, Peking University, Beijing 100871, China. E-mail: boshuai_mu@pku.edu.cn; zbliu@pku.edu.cn*

*[b]Peking University–Tsinghua University Center for Life Sciences, Peking University, Beijing 100871, China*

*[c]Changping Laboratory, Beijing 102206, China*

*[d]Key Laboratory of Carcinogenesis and Translational Research (Ministry of Education/Beijing), NMPA Key Laboratory for Research and Evaluation of Radiopharmaceuticals (National Medical Products Administration), Department of Nuclear Medicine, Peking University Cancer Hospital & Institute, Beijing 100142, China*

† Electronic supplementary information (ESI) available. See DOI: https://doi.org/10.1039/d4sc05558f

‡ These authors contributed equally to this work.

could compromise the cost-effectiveness and functional group compatibility.[5] Therefore, developing facile and effective methods that enable aerobic oxidation is always in high demand.

Ionizing radiation (*e.g.*, γ-ray photons), the main form of nuclear energy utilization,[6] has been widely applied in wastewater treatment,[7] material fabrication,[8] and radiotherapy.[9] These high-energy particles can uniformly and effectively produce highly reactive species, which can overcome activation barriers for subsequent reactions under ambient conditions. Furthermore, ionizing radiation possesses good penetrability and industrial accessibility, holding promise for large-scale production.[10] Recently, ionizing radiation has been harnessed to produce chemical feedstocks such as hydrogen,[11] methanol,[12] acetic acid,[13] and ammonia,[14] demonstrating the feasibility of nuclear energy-induced chemical transformations. To the best of our knowledge, radiation-induced aerobic oxidation has not yet been developed. Diverging from photochemical aerobic oxidation processes, in which photoresponsive groups harness ultraviolet-visible light energy to activate $O_2$, solvent molecules with the largest proportion predominantly absorb energy and trigger $O_2$ activation in radiation-induced aerobic oxidation reactions.[15] Upon irradiation, stable solvent molecules can be converted into solvated electrons $(e_{sol}^-)$, hydrogen radicals $(H\cdot)$, and solvent-derived radicals $(\cdot R_{sol})$ with a homogeneous distribution within tens of nanoseconds.[16] In the presence of air, $\cdot R_{sol}$ with a high radiolytic yield can rapidly activate $O_2$ $(k > 10^9 \text{ L mol}^{-1} \text{ s}^{-1})$ to generate solvent-derived peroxyl radicals $(R_{sol}OO\cdot)$.[17] As a group of ROS that have received little attention yet commonly exist in the radiolysis of various solvents, reactivity-adjustable $R_{sol}OO\cdot$ are anticipated to enable a broad array of aerobic oxidation reactions (Scheme 1b).

Herein, we used γ-ray radiation from a $^{60}$Co source to investigate whether ionizing radiation could induce aerobic oxidation processes. The results revealed that multiple $R_{sol}OO\cdot$ could successfully promote the oxidation of sulfides and phosphorus(III) compounds at ambient temperature and pressure without any catalysts. This aerobic oxidation strategy exhibits favorable functional group compatibility and is suitable for gram-scale synthesis, demonstrating that ionizing radiation can enable selective oxidation processes for synthesizing chemical feedstocks rather than unselectively degrading organics to carbon dioxide and water as in wastewater treatment. It provides an effective approach for organic synthesis and opens broad prospects for the valuable utilization of nuclear energy.
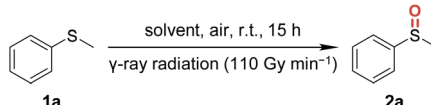
## Results and discussion

### Optimization of the reaction conditions

Sulfoxide is a ubiquitous structural building block widely applied in natural products, pharmaceuticals, agrochemicals, food additives, and other chemical feedstocks.[18] Normally, sulfoxides are produced through the oxidation of the corresponding sulfides with the help of various oxidants, such as *m*-chloroperbenzoic acid, oxone, hydrogen peroxide, *etc.*[19] To validate our hypothesis, we first selected methylphenyl sulfide (**1a**) as the model compound to investigate radiation-induced aerobic oxidation.

The initial reaction was carried out in different solvents under an air atmosphere and irradiated with γ-rays at room temperature with a dose rate of 110 Gy min$^{-1}$ (1 Gy = 1 J kg$^{-1}$) (Tables 1 and S1, ESI†). To our delight, acetonitrile ($CH_3CN$) as the solvent gave the highest yield of (methylsulfinyl)benzene (**2a**), reaching 95% after 15 h of irradiation (Table 1, entry 1). Methanol ($CH_3OH$), acetone, and ethyl acetate (EtOAc) could also facilitate the oxidation of **1a** in moderate yields (Table 1, entries 2–4), while tetrahydrofuran (THF), cyclohexane, dimethyl sulfoxide (DMSO), *N*,*N*-dimethylformamide (DMF), toluene, and dichloromethane ($CH_2Cl_2$) were not conducive to the reaction (Table 1, entries 5–10). Considering that the addition of water can inhibit the conversion of sulfoxides to sulfones through hydrogen bond interactions, we then evaluated a mixed solvent of $CH_3CN$ and water (Table 1, entries 11 and 12, and Table S2, ESI†).[20] However, with the increase in the proportion of water, the yield correspondingly decreased, which could be attributed to the decreased solubility of the substrate and the reduced concentration of the primary oxidizing species. In addition, hydroxyl radicals which are potent oxidants produced from water radiolysis tended to cause overoxidation of organics, thus reducing the yield. The dose rate had almost no effect on the reaction performance when the total absorbed dose was fixed (Table S3, ESI†). Of note, the reaction time played a vital role in determining the product distribution (Table S4, ESI†). We found that increasing the reaction time from 2 h to 15 h would raise the yield of **2a** from 27% to 95%. However, when the reaction time exceeded 15 h, **2a** started to convert to methylphenyl sulfone (**3a**), indicating that it is feasible to selectively obtain sulfoxides or sulfones by modulating the reaction time. When **2a** was used as the substrate, **3a** could also be obtained

**Table 1** Optimization of the reaction conditions$^a$



| Entry | Solvent | Yield$^b$ (%) |
|---|---|---|
| 1$^c$ | **CH$_3$CN** | **95** |
| 2 | CH$_3$OH | 87 |
| 3 | EtOAc | 62 |
| 4 | Acetone | 75 |
| 5 | THF | 18 |
| 6 | Cyclohexane | 22 |
| 7 | DMSO | Trace |
| 8 | DMF | 21 |
| 9 | Toluene | 24 |
| 10 | CH$_2$Cl$_2$ | n.d. |
| 11 | CH$_3$CN/H$_2$O (4/1) | 72 |
| 12 | CH$_3$CN/H$_2$O (1/4) | 16 |

$^a$ Reaction conditions: **1a** (0.3 mmol) in solvent (15 mL) with γ-ray radiation (dose rate: 110 Gy min$^{-1}$, measured using a Fricke dosimeter) at room temperature and under an air atmosphere for 15 h. $^b$ Determined by gas chromatography-mass spectrometry (GC-MS) using 1,3,5-trimethoxybenzene as the internal standard. $^c$ The optimized reaction condition. n.d. = no detected.

with the other reaction conditions unchanged, further demonstrating that sulfoxides served as necessary intermediates in the oxidation of sulfides to sulfones (Table S5, ESI†).

**Substrate scope**

Based on the optimized reaction conditions, we further evaluated the substrate scope of radiation-induced aerobic oxidation using various sulfides. Aryl methyl sulfide derivatives with

different substituents were examined first. As shown in Fig. 1, both electron-donating groups and electron-withdrawing groups were tolerated. Aryl methyl sulfides with electron-donating groups (*e.g.*, alkyl, alkoxy, and trifluoromethoxy) (**1b**–**1d**) were converted to the corresponding sulfoxides (**2b**–**2d**) in moderate yields. Similarly, aryl methyl sulfides with electron-withdrawing groups (*e.g.*, halogen, nitro, cyano, acetyl, and trifluoromethyl) (**1e**–**1s**) could also be converted to sulfoxides (**2e**–
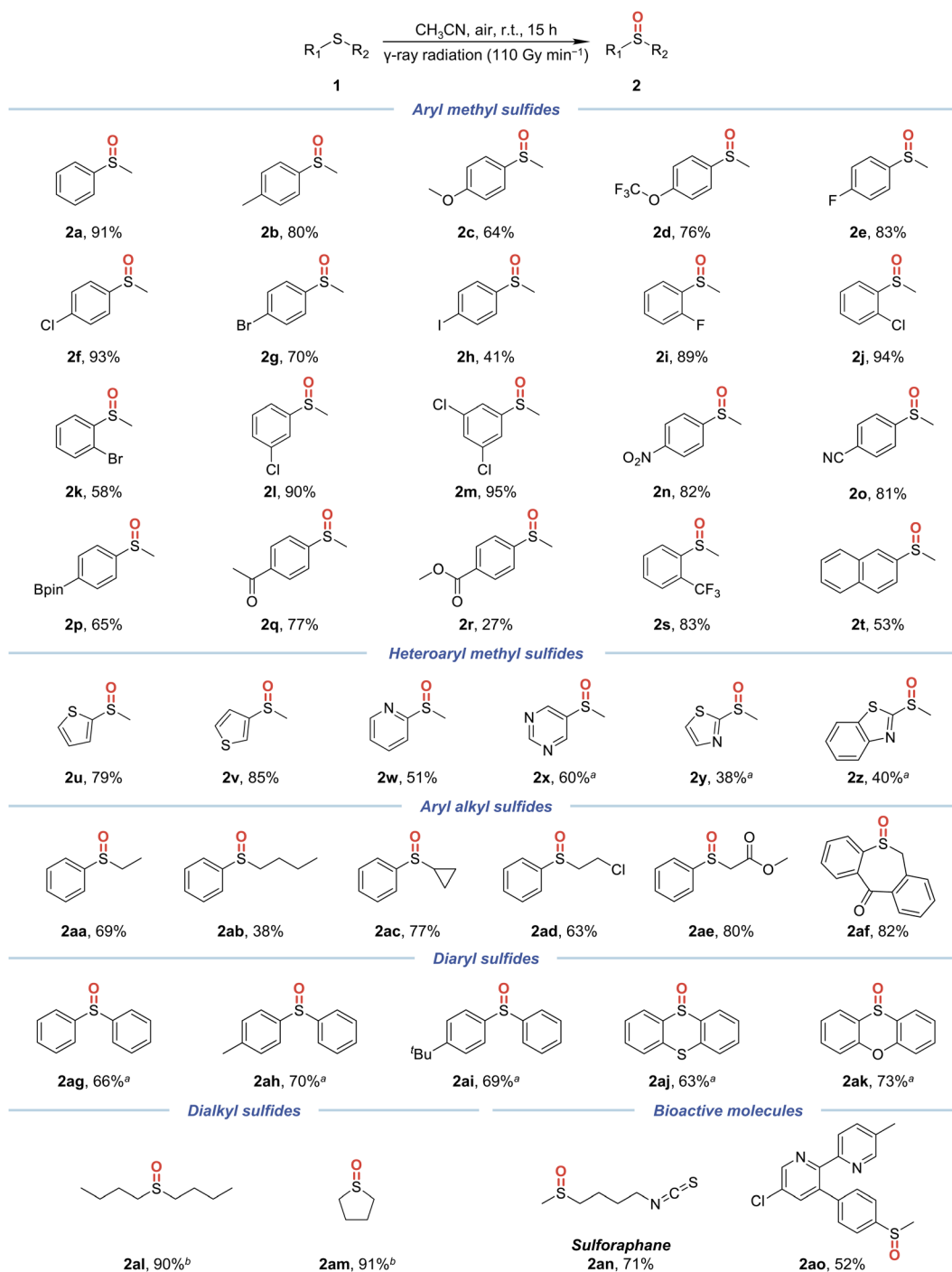


**Fig. 1** The substrate scope of radiation-induced aerobic oxidation of sulfides. Reaction conditions: **1** (0.3 mmol) in $CH_3CN$ (15 mL) with γ-ray radiation (dose rate: 110 Gy min$^{-1}$, measured using a Fricke dosimeter) at room temperature and under an air atmosphere for 15 h. All yields are isolated. [a]Reaction time: 30 h. [b]Reaction time: 7 h.

**2s**) in satisfactory yields. High functional group compatibility was shown by the successful preservation of various groups in products, including trifluoromethoxy (**2d**), nitro (**2n**), cyano (**2o**), boronic pinacol ester (Bpin, **2p**), and trifluoromethyl groups (**2s**). Additionally, the number and positional properties of the functional groups have a negligible effect on the reactivity (**2i–2m**). Next, we investigated the oxidation efficiency of naphthyl or heteroaryl methyl sulfides. To our satisfaction, sulfides bearing naphthalene (**2t**), thiophene (**2u** and **2v**), pyridine (**2w**), pyrimidine (**2x**), thiazole (**2y**), or benzothiazole (**2z**) were also accommodated by the radiation-induced aerobic oxidation system. It is worth mentioning that the sulfur-containing heteroaromatic rings remained unoxidized, showing that this oxidation strategy is chemoselective.

Subsequently, we expanded the substrate scope to other aryl alkyl sulfides with different chain lengths, isomeric structures, and functional groups. They could all be oxidized to sulfoxides with alkyl motifs retained in moderate yields (**2aa–2af**). Apart from aryl alkyl sulfides, a series of diaryl sulfides and dialkyl sulfides were evaluated. The relatively low reactivity of diaryl sulfides is attributed to the conjugation effect of benzene rings (**2ag–2ak**). Considering that thianthrene contains two sulfur atoms, we found that only mono-oxygenation sulfoxide (**2aj**) could be obtained. In contrast to diaryl sulfides, dialkyl sulfides could be transformed into sulfoxides (**2al** and **2am**) in excellent yields in a shorter reaction time. The above results indicate that electronic effects of the substituents linked to the sulfur atom play an important role in the conversion efficiency. The conversion of sulfides containing electron-donating groups was easier than those bearing electron-withdrawing groups. In addition, diaryl sulfides required a longer reaction time than aryl alkyl sulfides and dialkyl sulfides due to the decreased electron density on the sulfur atom.

Encouraged by the satisfactory results above, we further verified the applicability of this oxidation strategy for synthesizing bioactive molecules and pharmaceuticals. A potential anticancer drug sulforaphane (**2an**) was obtained in 71% yield with its sensitive isothiocyanate group preserved.[21] Moreover, the corresponding sulfoxide of etoricoxib (**2ao**), a cyclooxygenase (COX)-2 inhibitor, could also be prepared in 52% yield.[22]

Similar to the sulfur atoms in sulfides, the phosphorus atoms in phosphorus(III) compounds also tend to accept oxygen atoms and be oxidized to form the corresponding phosphorus(V)



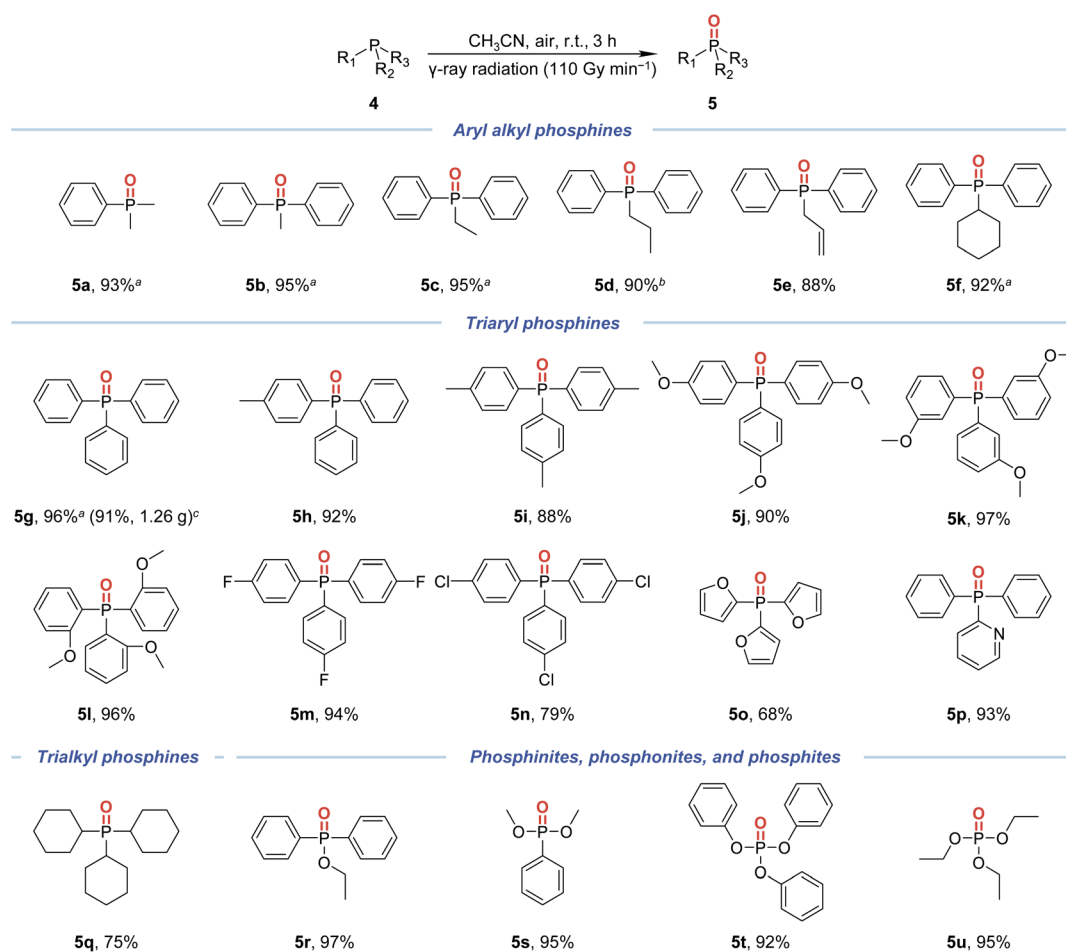**Fig. 2** The substrate scope of radiation-induced aerobic oxidation of phosphorus(III) compounds. Reaction conditions: **4** (0.3 mmol) in CH$_3$CN (15 mL) with γ-ray radiation (dose rate: 110 Gy min$^{-1}$, measured using a Fricke dosimeter) at room temperature and under an air atmosphere for 3 h. All yields are isolated. [a]Reaction time: 100 min. [b]Reaction time: 220 min. [c]Gram-scale synthesis.

compounds, which are crucial for the synthesis of organophosphorus compounds.[23] As shown in Fig. 2, aryl alkyl phosphine oxides with different alkyl motifs (**5a–5f**), triaryl phosphine oxides with different substituents (**5g–5p**), and tricyclohexylphosphine oxide (**5q**) could all be readily obtained with excellent yields in a much shorter reaction time. Alkene (**5e**), furan ring (**5o**), and pyridine ring (**5p**) were well preserved after the reaction. Of note, **5g** was successfully obtained at a gram-scale level (91%, 1.26 g), suggesting that this protocol is promising for scale-up synthesis. Moreover, this radiation-induced aerobic oxidation strategy could also be applied to the synthesis of phosphinates, phosphonates, and phosphates (**5r–5u**).

### Mechanistic investigation

We next turned our attention to the mechanism of radiation-induced aerobic oxidation of sulfides and phosphorus(III) compounds. All mechanistic studies were conducted with **1a** as the model substrate and $CH_3CN$ as the solvent. According to the results of control experiments, both γ-ray radiation and $O_2$ were essential for the success of this oxidation strategy (Fig. 3a). Then, we introduced the ROS fluorescent probe 2′,7′-dichlorodihydrofluorescein (DCFH) to the system and observed an increased fluorescence signal with prolonged irradiation time, supporting the generation of ROS in this oxidation process (Fig. S2, ESI†).

To further investigate the key ROS, a series of quenching experiments were performed by introducing various scavengers (Fig. 3b). When an electron quencher (e.g., $AgNO_3$) was added, there was no significant difference in the reaction performance, demonstrating that $e_{sol}^-$ and $O_2^{\bullet-}$ derived from $e_{sol}^-$ were not the primary reactive species. Similarly, we utilized the $O_2^{\bullet-}$-specific probe nitrotetrazolium blue chloride (NBT) to monitor the superoxide species, and the unabated absorbance at 260 nm revealed the absence of $O_2^{\bullet-}$ (Fig. S3, ESI†). By introducing diphenyl sulfoxide ($Ph_2SO$), we could rule out the formation of a persulfoxide intermediate between sulfide and $^1O_2$ in that the reaction performance remained essentially unchanged and only a trace amount of diphenyl sulfone ($Ph_2SO_2$) formed between persulfoxide and $Ph_2SO$ (Fig. S4, ESI†).[24] Meanwhile, the reaction performance was hardly affected when deuterated acetonitrile ($CD_3CN$) was used as the solvent, where the lifetime of $^1O_2$ is longer [$\tau_\Delta(CD_3CN/CH_3CN) = 1625/82$ μs] (Fig. S7, ESI†).[25] Therefore, we speculated that $^1O_2$ also played a minor role in this oxidation process. The addition of 1,4-dimethoxybenzene (DMB) as a sulfide radical cation ($R_2S^{\bullet+}$) scavenger also did not significantly suppress the reaction, suggesting that $R_2S^{\bullet+}$ might not be as important as they are in photocatalytic aerobic oxidation driven by $O_2^{\bullet-}$ or $^1O_2$.[26] Hydroxyl radicals (·OH) were excluded by introducing 2-propanol (i-PrOH) as the scavenger. Furthermore, when 2,2,6,6-tetramethyl-1-piperinedinyloxy (TEMPO) or butylated hydroxytoluene (BHT) was added as the radical trapping reagent, the oxidation of **1a** was severely suppressed, and the adduct with the cyanomethyl radical (·CH_2CN) **6** or **7** could be observed by high-resolution mass spectrometry (HRMS) (Fig. 3c, d, and S5, ESI†). These results indicated that a ·CH_2CN-mediated radical process may be involved.
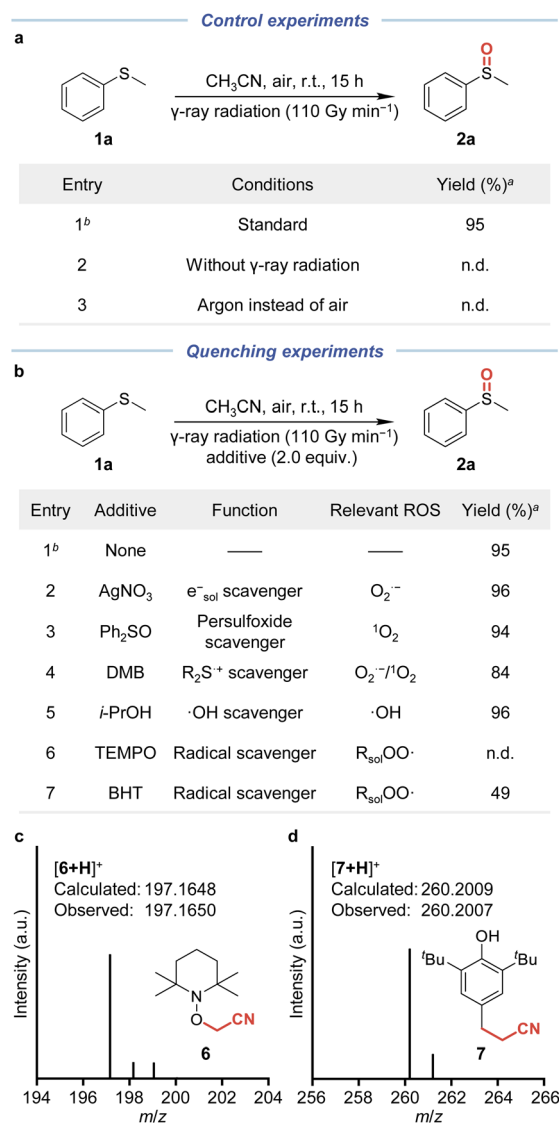


Fig. 3 Experiments for mechanistic investigation. (a) Control experiments for mechanistic studies. (b) Quenching experiments for investigating the key ROS. (c) High-resolution mass spectrometry of the adduct between TEMPO and ·CH_2CN. (d) High-resolution mass spectrometry of the adduct between BHT and ·CH_2CN. [a]Determined by GC-MS using 1,3,5-trimethoxybenzene as the internal standard. [b]Standard conditions: **1a** (0.3 mmol) in $CH_3CN$ (15 mL) with γ-ray radiation (dose rate: 110 Gy min$^{-1}$, measured using a Fricke dosimeter) at room temperature and under an air atmosphere for 15 h. n.d. = no detected.

**Control experiments**

| Entry | Conditions | Yield (%)[a] |
|---|---|---|
| 1[b] | Standard | 95 |
| 2 | Without γ-ray radiation | n.d. |
| 3 | Argon instead of air | n.d. |

**Quenching experiments**

| Entry | Additive | Function | Relevant ROS | Yield (%)[a] |
|---|---|---|---|---|
| 1[b] | None | —— | —— | 95 |
| 2 | $AgNO_3$ | $e_{sol}^-$ scavenger | $O_2^{\bullet-}$ | 96 |
| 3 | $Ph_2SO$ | Persulfoxide scavenger | $^1O_2$ | 94 |
| 4 | DMB | $R_2S^{\bullet+}$ scavenger | $O_2^{\bullet-}/^1O_2$ | 84 |
| 5 | i-PrOH | ·OH scavenger | ·OH | 96 |
| 6 | TEMPO | Radical scavenger | $R_{sol}OO\bullet$ | n.d. |
| 7 | BHT | Radical scavenger | $R_{sol}OO\bullet$ | 49 |

Based on the above results, we propose that the radiation-induced aerobic oxidation process differs from most photocatalytic processes mediated by $O_2^{\bullet-}$ or $^1O_2$. Solvent-derived peroxyl radicals (e.g., cyanomethylperoxyl radicals, ·OOCH_2-CN) generated from the rapid combination of $O_2$ and ·$R_{sol}$ (e.g., ·CH_2CN) may enable this oxidation process.

To further unravel the mechanism, density functional theory (DFT) calculations were performed on the model substrate **1a** with $CH_3CN$ as the solvent. The proposed mechanism and calculated results are shown in Fig. 4. Upon irradiation with $^{60}Co$ γ-rays, $CH_3CN$ is initially ionized to generate $e^-$ and
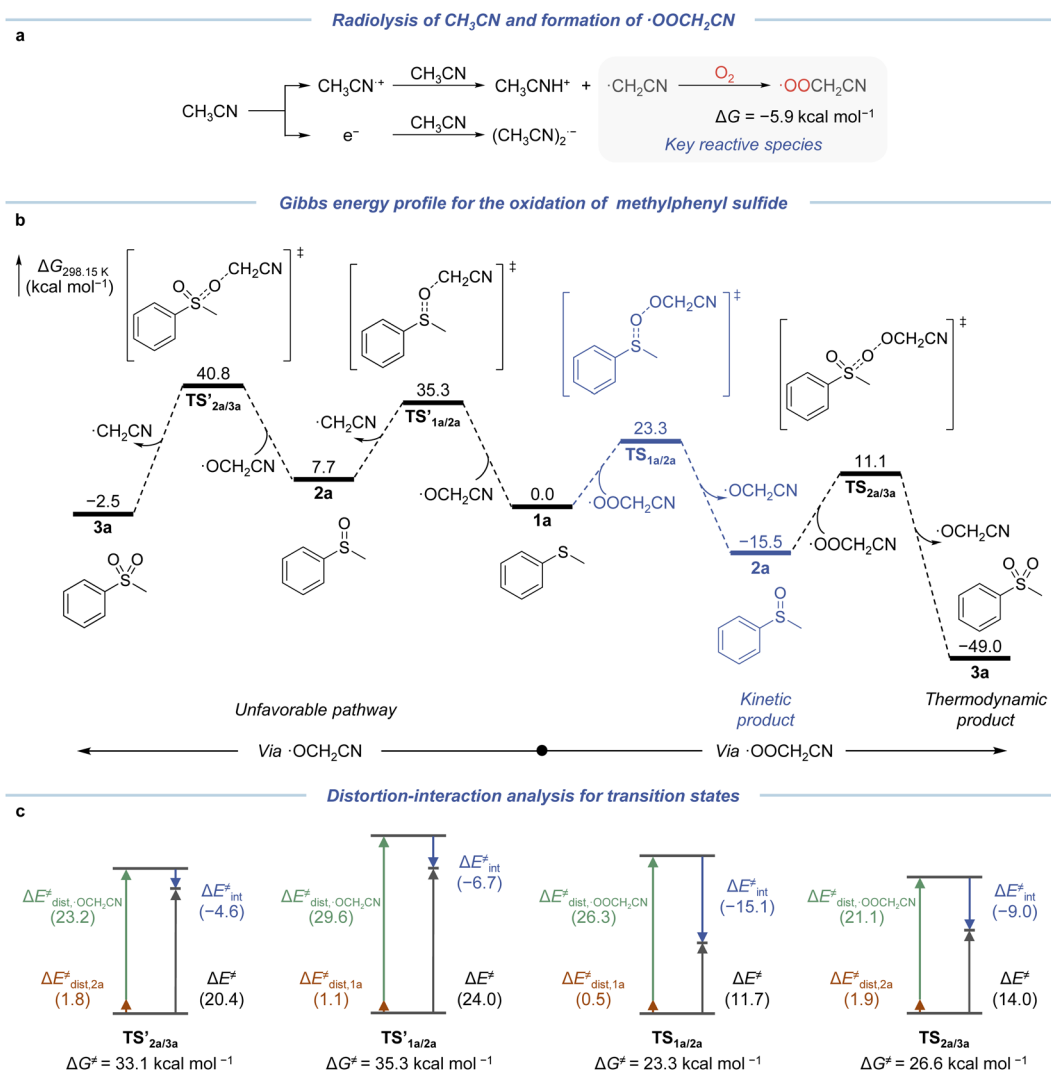
**Fig. 4** Mechanism proposal and DFT calculations. (a) The radiolysis of $CH_3CN$ and the formation of $\cdot OOCH_2CN$. (b) Gibbs energy profile for the radiation-induced aerobic oxidation of **1a** to **2a** and **3a** via $\cdot OCH_2CN$ (left) or $\cdot OOCH_2CN$ (right) was calculated at the B3LYP-D3/6-311+G(d,p)/SMD(acetonitrile) level of theory. (c) Distortion–interaction analysis for transition states in the Gibbs energy profile was calculated at the B3LYP-D3/6-311+G(d,p)/SMD(acetonitrile) level of theory.

radical cations $(CH_3CN^{\cdot+})$ along the tracks. After the subsequent rapid processes such as spur expansion, geminate recombination, and intra-track reaction, $\cdot CH_2CN$ becomes the predominant reactive species in the solution within tens of nanoseconds.[27] Therefore, the cleavage of the C–H bond is not the rate-determining step, which is consistent with the findings of kinetic studies (Fig. S7, ESI†). According to previous studies and the calculated results, once $\cdot CH_2CN$ is formed, it reacts with $O_2$ to produce $\cdot OOCH_2CN$ smoothly ($k = 1.3 \times 10^9$ L mol$^{-1}$ s$^{-1}$), which is spontaneous (Fig. 4a and S8, ESI†).[28] The $\cdot OOCH_2CN$ then undergoes the oxygen atom transfer (OAT) process with **1a** to yield **2a** via $TS_{1a/2a}$ with the Gibbs activation energy ($\Delta G^{\neq}$) and the Gibbs reaction energy ($\Delta G$) being 23.3 kcal mol$^{-1}$ and −15.5 kcal mol$^{-1}$, respectively. By contrast, it is more difficult for $\cdot OOCH_2CN$ to undergo the same process with **2a** to produce **3a** via $TS_{2a/3a}$, where $\Delta G^{\neq}$ and $\Delta G$ are 26.6 kcal mol$^{-1}$ and −33.5 kcal mol$^{-1}$. These results reveal that

sulfoxides are kinetic products and sulfones are thermodynamic products, which is consistent with the relationship between product distribution and reaction time (Table S4, ESI†). Moreover, the second oxygen atom of $\cdot OOCH_2CN$ is unlikely to undergo the OAT process, because the values of $\Delta G^{\neq}$ for the reaction of cyanomethoxy radicals ($\cdot OCH_2CN$) with **1a** and **2a** are as high as 35.3 kcal mol$^{-1}$ and 33.1 kcal mol$^{-1}$, respectively, indicating that the $\cdot OCH_2CN$ pathway is unfavorable compared to the $\cdot OOCH_2CN$ pathway (Fig. 4b). All of the transition state geometries were determined by intrinsic reaction coordinate (IRC) analysis (Fig. S9, ESI†).

Distortion–interaction analysis was also performed on these four transition states to explain why $\cdot OOCH_2CN$ is more conducive to undergoing the OAT process (Fig. 4c and Table S8, ESI†).[29] Compared to the other three transition states, the total distortion energy ($\Delta E^{\neq}_{dist}$, the energy required to distort substrate and oxidizing species into the transition state
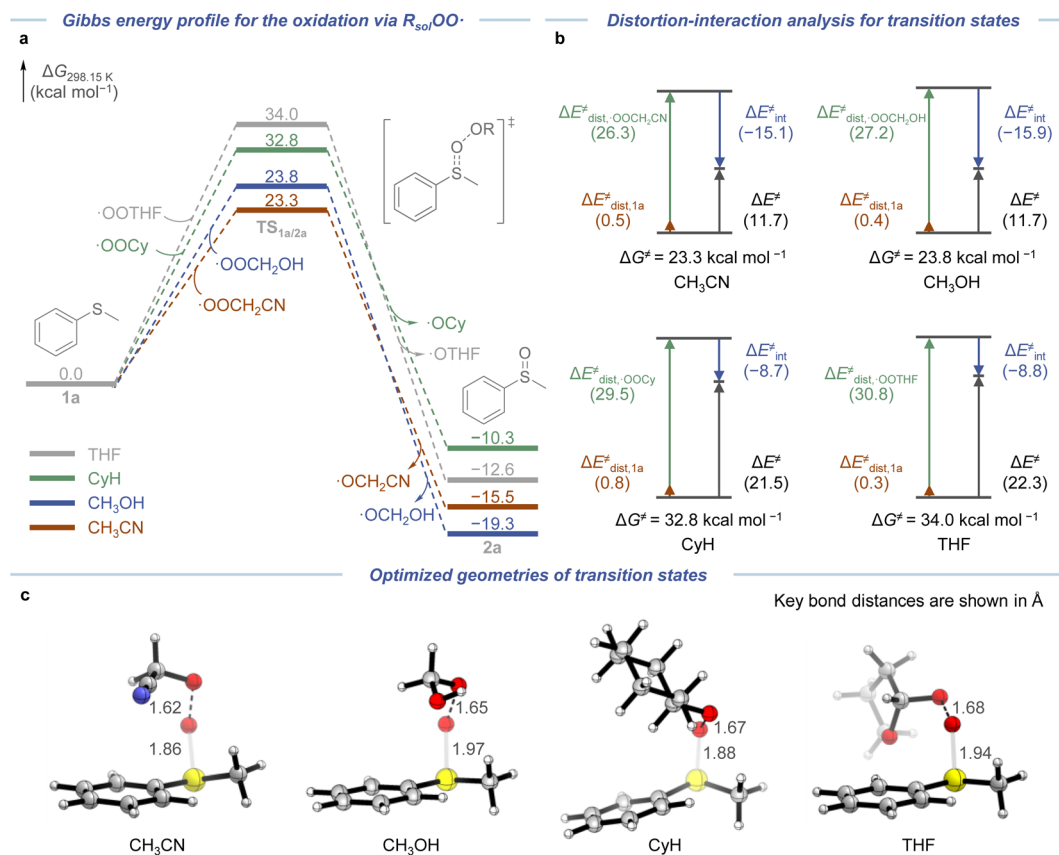
**Fig. 5** Multiple solvent-derived peroxyl radicals enable the radiation-induced aerobic oxidation strategy. (a) Gibbs energy profile for the radiation-induced aerobic oxidation of **1a** to **2a** *via* different $R_{sol}OO\cdot$ was calculated at the B3LYP-D3/6-311+G(d,p)/SMD level of theory. CyH = cyclohexane. (b) Distortion–interaction analysis for transition states in the Gibbs energy profile was calculated at the B3LYP-D3/6-311+G(d,p)/SMD level of theory. (c) Optimized geometries of transition states.

geometry) of $TS_{1a/2a}$ is 26.8 kcal mol$^{-1}$, which is higher than that of $TS_{2a/3a}$ and $TS'_{2a/3a}$. However, the interaction energy ($\Delta E^{\neq}_{int}$, the energy released when the two fragments form a complete transition state) of $TS_{1a/2a}$ is down to $-15.1$ kcal-mol$^{-1}$, which compensates for the relatively higher $\Delta E^{\neq}_{dist}$. Therefore, the activation energy ($\Delta E^{\neq}$, the sum of $\Delta E^{\neq}_{dist}$ and $\Delta E^{\neq}_{int}$) of $TS_{1a/2a}$ is the lowest (11.7 kcal mol$^{-1}$), suggesting that $TS_{1a/2a}$ is relatively stable and the transformation from **1a** to **2a** *via* $\cdot OOCH_2CN$ is more favorable.

Similar to $\cdot CH_2CN$, hydroxymethyl radicals ($\cdot CH_2OH$), cyclohexyl radicals ($\cdot C_6H_{11}$), and tetrahydrofuran-2-yl radicals ($\cdot C_4H_7O$) generated from solvent radiolysis could also react with O$_2$ rapidly to produce the corresponding peroxyl radicals, which then promote the oxidation of **1a** to **2a** through the OAT process.[30] The results of control experiments and radical trapping experiments showed that γ-ray radiation, O$_2$, and $\cdot R_{sol}$ also play important roles in radiation-induced aerobic oxidation mediated by other several solvents (Tables S6, S7 and Fig. S6, ESI†). As shown in Fig. 5a, as the peroxyl radicals change from $\cdot OOCH_2CN$, hydroxymethylperoxyl radicals ($\cdot OOCH_2OH$), and cyclohexylperoxyl radicals ($\cdot OOCy$) to tetrahydrofuran-2-peroxy radicals ($\cdot OOTHF$), the value of $\Delta G^{\neq}$ increases from 23.3 kcal mol$^{-1}$ to 34.0 kcal mol$^{-1}$, which indicates that the OAT

process becomes difficult to proceed. This trend is also consistent with the reaction performance shown in Table 1. The yield of **2a** decreases with the increase in Gibbs activation energy, indicating that the oxygen atom transfer ability of $R_{sol}OO\cdot$ is a key factor affecting the reaction performance. Distortion–interaction analysis reveals that the interaction between the substrate and $R_{sol}OO\cdot$ is particularly important for the stabilization of the transition state (Fig. 5b and Table S8, ESI†). When the values of $\Delta E^{\neq}_{dist}$ are nearly identical, the value of $\Delta E^{\neq}_{int}$ in CH$_3$CN ($-15.1$ kcal mol$^{-1}$) or CH$_3$OH ($-15.9$ kcal mol$^{-1}$) is significantly lower compared to that in cyclohexane ($-8.7$ kcal mol$^{-1}$) or THF ($-8.8$ kcal mol$^{-1}$), contributing to a more stable transition state and a lower $\Delta E^{\neq}$ (11.7 kcal mol$^{-1}$). The unfavorable interaction between $\cdot OOCy$ or $\cdot OOTHF$ and **1a** may be due to the steric hindrance brought by the cyclohexyl or tetrahydrofuran-2-yl group (Fig. 5c). Therefore, the efficacy of the radiation-induced aerobic oxidation strategy heavily relies on the solvent type and the reactive species generated from solvent radiolysis.

## Conclusions

In summary, we presented an ionizing radiation-induced aerobic oxidation strategy that enables the selective oxidation

of sulfides and phosphorus(III) compounds at room temperature without catalysts. This strategy exhibited a wide substrate scope and favorable functional group compatibility. Through mechanistic experiments and DFT calculations, we established that highly active $R_{sol}OO\cdot$ produced from solvent radiolysis, rather than $O_2^{\cdot-}$, $^1O_2$, and $\cdot OH$, serve as the primary oxidizing species and facilitate the oxidation through an OAT process. Notably, $R_{sol}OO\cdot$ are commonly generated during the radiolysis of various solvents in the presence of $O_2$, making it easy to adjust the reaction performance by choosing the appropriate solvent. Combined with the increasing accessibility and strong penetrability of ionizing radiation, our aerobic oxidation strategy is expected to have a wider range of applications in various oxidation reactions and scale-up synthesis, presenting a fresh avenue for nuclear energy utilization.

## Data availability

The ESI† includes details of optimization studies, substrate scope studies, mechanistic studies, and computational studies. Characterization data, NMR spectra, and Cartesian coordinates of all optimized geometries are included as well.

## Author contributions

Z. L. conceived the study. Y. X., assisted by B. M., W. L. and J. L., performed optimization studies and substrate scope studies. Y. X., assisted by B. M. and Z. T., performed mechanistic studies. Y. X., assisted by B. M. and Z. S., performed computational studies. Y. X., B. M. and Z. L. analyzed the data. Z. L. wrote the paper with inputs from all authors. All authors discussed the results and commented on the paper.

## Conflicts of interest

There are no conflicts to declare.

## Acknowledgements

## Notes and references

1 (a) T. Punniyamurthy, S. Velusamy and J. Iqbal, *Chem. Rev.*, 2005, **105**, 2329–2364; (b) S. Ma, J. Liu, S. Li, B. Chen, J. Cheng, J. Kuang, Y. Liu, B. Wan, Y. Wang, J. Ye, Q. Yu, W. Yuan and S. Yu, *Adv. Synth. Catal.*, 2011, **353**, 1005–1017; (c) X. Jiang, J. Zhang and S. Ma, *J. Am. Chem. Soc.*, 2016, **138**, 8344–8347.

2 (a) Z. Shi, C. Zhang, C. Tang and N. Jiao, *Chem. Soc. Rev.*, 2012, **41**, 3381–3430; (b) Y. Liang, J. Wei, X. Qiu and N. Jiao, *Chem. Rev.*, 2018, **118**, 4912–4945; (c) C. Tang, X. Qiu, Z. Cheng and N. Jiao, *Chem. Soc. Rev.*, 2021, **50**, 8067–8101.

3 X. Zhang, K. P. Rakesh, L. Ravindar and H.-L. Qin, *Green Chem.*, 2018, **20**, 4790–4833.

4 (a) D. M. Schultz and T. P. Yoon, *Science*, 2014, **343**, 1239176; (b) J. Wei, J. Meng, C. Zhang, Y. Liu and N. Jiao, *Nat. Commun.*, 2024, **15**, 1886.

5 E. Skolia, P. L. Gkizis, N. F. Nikitas and C. G. Kokotos, *Green Chem.*, 2022, **24**, 4108–4118.

6 (a) J. Parsons, J. Buongiorno, M. Corradini and D. Petti, *Science*, 2019, **363**, 105; (b) M. M. Ramirez-Corredores, L. A. Diaz, A. M. Gaffney and C. A. Zarzana, *Renew. Sustain. Energy Rev.*, 2021, **150**, 111450.

7 (a) A. V. Ponomarev and B. G. Ershov, *Environ. Sci. Technol.*, 2020, **54**, 5331–5344; (b) K. Londhe, C.-S. Lee, Y. Zhang, S. Grdanovska, T. Kroc, C. A. Cooper and A. K. Venkatesan, *ACS EST Eng.*, 2021, **1**, 827–841.

8 (a) Z. Zhang, X. Cui, W. Yuan, Q. Yang, H. Liu, H. Xu and H.-L. Jiang, *Inorg. Chem. Front.*, 2018, **5**, 29–38; (b) K. Guo, A. Baidak and Z. Yu, *J. Mater. Chem. A*, 2020, **8**, 23029–23058; (c) J. Chen, M. Zhang, J. Shu, M. Yuan, W. Yan, P. Bai, L. He, N. Shen, S. Gong, D. Zhang, J. Li, J. Hu, R. Li, G. Wu, Z. Chai, J. Yu and S. Wang, *Angew. Chem., Int. Ed.*, 2021, **60**, 14858–14863; (d) J. Chen, M. Zhang, S. Zhang, K. Cao, X. Mao, M. Zhang, L. He, X. Dong, J. Shu, H. Dong, F. Zhai, R. Shen, M. Yuan, X. Zhao, G. Wu, Z. Chai and S. Wang, *Angew. Chem., Int. Ed.*, 2022, **61**, e202212532.

9 (a) K. Ni, G. Lan, Y. Song, Z. Hao and W. Lin, *Chem. Sci.*, 2020, **11**, 7641–7653; (b) Q. Fu, H. Li, D. Duan, C. Wang, S. Shen, H. Ma and Z. Liu, *Angew. Chem., Int. Ed.*, 2020, **59**, 21546–21552; (c) Z. Ding, Z. Guo, Y. Zheng, Z. Wang, Q. Fu and Z. Liu, *J. Am. Chem. Soc.*, 2022, **144**, 9458–9464; (d) Z. Guo, H. Hong, Y. Zheng, Z. Wang, Z. Ding, Q. Fu and Z. Liu, *Angew. Chem., Int. Ed.*, 2022, **61**, e202205014; (e) D. Duan, Y. Han, Z. Tu, H. Guo, Z. Zhang, Y. Shi, J. Li, Q. Sun, J. Chen, Z. Li, T. Liu, D. Cui and Z. Liu, *CCS Chem.*, 2023, **5**, 2589–2602; (f) Q. Fu, Z. Gu, S. Shen, Y. Bai, X. Wang, M. Xu, P. Sun, J. Chen, D. Li and Z. Liu, *Nat. Chem.*, 2024, **16**, 1348–1356; (g) T. Luo, X. Jiang, Y. Fan, E. Yuan, J. Li, L. Tillman and W. Lin, *Natl. Sci. Rev.*, 2024, **11**, nwae167; (h) Q. Fu, S. Zhang, S. Shen, Z. Gu, J. Chen, D. Song, P. Sun, C. Wang, Z. Guo, Y. Xiao, Y. Q. Gao, Z. Guo and Z. Liu, *Nat. Biomed. Eng.*, 2024, **8**, 1425–1435.

10 (a) M. Zhang, J. Chen, S. Zhang, X. Zhou, L. He, M. V. Sheridan, M. Yuan, M. Zhang, L. Chen, X. Dai, F. Ma, J. Wang, J. Hu, G. Wu, X. Kong, R. Zhou, T. E. Albrecht-Schmitt, Z. Chai and S. Wang, *J. Am. Chem. Soc.*, 2020, **142**, 9169–9174; (b) J. Chen, M. Zhang, J. Shu, S. Liu, X. Dong, C. Li, L. He, M. Yuan, Y. Wu, J. Xu, D. Zhang, F. Ma, G. Wu, Z. Chai and S. Wang, *J. Am. Chem. Soc.*, 2023, **145**, 23651–23658.

11  C. Hu, L. Cheng, L. Zhou, Z. Jiang, P. Gan, S. Cao, Q. Li, C. Chen, Y. Wang, M. Mostafavi, S. Wang and J. Ma, *J. Am. Chem. Soc.*, 2023, **145**, 5578–5588.

12  C. Hu, Z. Jiang, Q. Wu, S. Cao, Q. Li, C. Chen, L. Yuan, Y. Wang, W. Yang, J. Yang, J. Peng, W. Shi, M. Zhai, M. Mostafavi and J. Ma, *Nat. Commun.*, 2023, **14**, 4767.

13  (*a*) F. Fang, X. Sun, Y. Liu and W. Huang, *J. Am. Chem. Soc.*, 2024, **146**, 8492–8499; (*b*) B.-S. Mu, Y. Zhang, M. Peng, Z. Tu, Z. Guo, S. Shen, Y. Xu, W. Liang, X. Wang, M. Wang, D. Ma and Z. Liu, *Angew. Chem., Int. Ed.*, 2024, **63**, e202407443.

14  B.-S. Mu, Y. Xu, Z. Tu, Z. Yang, W. Liang, J. Li, X. Wang, S. Shen, J. Chen and Z. Liu, *Natl. Sci. Rev.*, 2024, **11**, nwae302.

15  E. Alizadeh and L. Sanche, *Chem. Rev.*, 2012, **112**, 5578–5602.

16  C. D. Jonah and B. S. M. Rao, *Radiation Chemistry: Present Status and Future Trends*, Elsevier Science, Amsterdam, 2001.

17  (*a*) B. Maillard, K. U. Ingold and J. C. Scaiano, *J. Am. Chem. Soc.*, 1983, **105**, 5095–5099; (*b*) S. L. Boyd, R. J. Boyd and L. R. C. Barclay, *J. Am. Chem. Soc.*, 1990, **112**, 5724–5730.

18  (*a*) C. Jacob, *Nat. Prod. Rep.*, 2006, **23**, 851–863; (*b*) N. Wang, P. Saidhareddy and X. Jiang, *Nat. Prod. Rep.*, 2020, **37**, 246–275.

19  (*a*) B. Yu, A.-H. Liu, L.-N. He, B. Li, Z.-F. Diao and Y.-N. Li, *Green Chem.*, 2012, **14**, 957–962; (*b*) R. D. Chakravarthy, V. Ramkumar and D. K. Chand, *Green Chem.*, 2014, **16**, 2190–2196; (*c*) X. Lang, W. R. Leow, J. Zhao and X. Chen, *Chem. Sci.*, 2015, **6**, 1075–1082; (*d*) X. Lang, W. Hao, W. R. Leow, S. Li, J. Zhao and X. Chen, *Chem. Sci.*, 2015, **6**, 5000–5005; (*e*) Y. Li, S. A.-e.-A. Rizvi, D. Hu, D. Sun, A. Gao, Y. Zhou, J. Li and X. Jiang, *Angew. Chem., Int. Ed.*, 2019, **58**, 13499–13506; (*f*) E. Skolia, P. L. Gkizis and C. G. Kokotos, *ChemPlusChem*, 2022, **87**, e202200008.

20  P. Pitchen, E. Dunach, M. N. Deshmukh and H. B. Kagan, *J. Am. Chem. Soc.*, 1984, **106**, 8188–8193.

21  J. D. Clarke, R. H. Dashwood and E. Ho, *Cancer Lett.*, 2008, **269**, 291–304.

22  D. J. Cochrane, B. Jarvis and G. M. Keating, *Drugs*, 2002, **62**, 2637–2651.

23  J.-Q. Zhang and L.-B. Han, *J. Org. Chem.*, 2024, **89**, 2090–2103.

24  (*a*) F. Jensen, A. Greer and E. L. Clennan, *J. Am. Chem. Soc.*, 1998, **120**, 4439–4449; (*b*) E. Baciocchi, T. D. Giacco, F. Elisei, M. F. Gerini, M. Guerra, A. Lapi and P. Liberali, *J. Am. Chem. Soc.*, 2003, **125**, 16444–16454.

25  R. L. Jensen, J. Arnbjerg and P. R. Ogilby, *J. Am. Chem. Soc.*, 2010, **132**, 8098–8105.

26  X.-N. Zou, D. Zhang, T.-X. Luan, Q. Li, L. Li, P.-Z. Li and Y. Zhao, *ACS Appl. Mater. Interfaces*, 2021, **13**, 20137–20144.

27  D. C. Grills and S. V. Lymar, *Phys. Chem. Chem. Phys.*, 2018, **20**, 10011–10017.

28  (*a*) S. Mosseri, P. Neta and D. Meisel, *Radiat. Phys. Chem.*, 1990, **36**, 683–687; (*b*) T. Imamura, T. Sumiyoshi, K. Takahashi and Y. Sasaki, *J. Phys. Chem.*, 1993, **97**, 7786–7791.

29  (*a*) F. Liu, R. S. Paton, S. Kim, Y. Liang and K. N. Houk, *J. Am. Chem. Soc.*, 2013, **135**, 15642–15649; (*b*) S. Chen, X. Huang, E. Meggers and K. N. Houk, *J. Am. Chem. Soc.*, 2017, **139**, 17902–17907.

30  (*a*) S. U. Choi and N. N. Lichtin, *J. Am. Chem. Soc.*, 1964, **86**, 3948–3953; (*b*) J. Kuruc and F. Šeršeň, *J. Radioanal. Nucl. Chem.*, 1990, **145**, 197–204; (*c*) G. R. Freeman, *J. Chem. Phys.*, 1960, **33**, 71–78.